III European Conference on Computational Mechanics
Solids, Structures and Coupled Problems in Engineering
C.A. Mota Soares et.al. (eds.)
Lisbon, Portugal, 5–9 June 2006

DEVELOPMENT OF A DEGRADATION MODEL FOR THE COLLAPSE ANALYSIS OF COMPOSITE AEROSPACE STRUCTURES

Adrian C. Orifici[1], Rodney S. Thomson[2], Richard Degenhardt[3], Chiara Bisagni[4] and Javid Bayandor[5]

[1] School of Aerospace, Mechanical & Manufacturing Engineering
Royal Melbourne Institute of Technology, GPO Box 2476V, Melbourne, Victoria, 3001, Australia
e-mail: s2008675@student.rmit.edu.au

[2] Cooperative Research Centre for Advanced Composite Structures Limited
506 Lorimer Street, Fishermans Bend, Victoria, 3207, Australia

[3] Institute of Composite Structures and Adaptive Systems, DLR – German Aerospace Center
Lilienthalplatz 7, 38108 Braunschweig, Germany

[4] Dipartimento di Ingegneria Aerospaziale, Politecnico di Milano,
Via La Masa 34, 20156 Milano, Italy

[5] The Sir Lawrence Wackett Aerospace Centre
School of Aerospace, Mechanical & Manufacturing Engineering
Royal Melbourne Institute of Technology, GPO Box 2476V, Melbourne, Victoria, 3001, Australia

Keywords: Composite, skin-stiffener separation, VCCT element, DCB, COCOMAT.

Abstract. *For stiffened structures in compression the most critical damage mechanism leading to structural collapse is delamination or adhesive disbonding between the skin and stiffener. This paper presents the development of a numerical approach capable of simulating interlaminar crack growth in composite structures as a representation of this damage mechanism. A degradation methodology was proposed using shell layers connected at the nodes by user-defined multiple point constraints (MPCs), and then controlling the properties of these MPCs to simulate the initiation and propagation of delamination and disbonding. A fracture mechanics approach based on the Virtual Crack Closure Technique (VCCT) is used to detect growth at the delamination front. Numerical predictions using the degradation methodology were compared to experimental results for double cantilever beam (DCB) specimens to demonstrate the effectiveness of the current approach. Future development will focus on addressing the apparent conservatism of the VCCT approach, and extending the application of the method to other specimen types and stiffened structures representative of composite fuselage designs. This work is part of the European Commission Project COCOMAT (Improved MATerial Exploitation at Safe Design of COmposite Airframe Structures by Accurate Simulation of COllapse), an ongoing four-year project that aims to exploit the large strength reserves of composite aerospace structures through more accurate prediction of collapse.*

1 INTRODUCTION

The European Commission Project COCOMAT (Improved **MAT**erial Exploitation at Safe Design of **CO**mposite Airframe Structures by Accurate Simulation of **CO**llapse) is an ongoing four-year project that aims to exploit the large strength reserves of composite aerospace structures through more accurate prediction of collapse [1,2]. Accordingly, one of the COCOMAT work-packages involves the development of degradation models capable of capturing the composite damage mechanisms that contribute to structural collapse. For stiffened structures in compression the most critical damage mechanism leading to structural collapse is detachment of the skin and stiffener, typically initiated at a stiffener flange edge. In order to include the effects of skin-stiffener separation into numerical analysis it is necessary to capture both the initiation and propagation of this type of damage. The work in this paper is on the growth of an existing skin-stiffener separation, with the prediction of damage initiation from an intact structure to be the subject of future work.

In structures manufactured from laminated composite materials, the phenomenon of skin-stiffener separation is analogous to that of interlaminar cracking, for which the use of fracture mechanics to predict crack growth has become common practice over the past two decades [3,4]. In fracture mechanics, the strain energy released in crack growth is compared to a threshold maximum strain energy release rate, called the interlaminar fracture toughness G_C. The strain energy release rate G is typically split into three components according to the separate mechanisms of crack growth: (I) opening in tension; (II) sliding in shear, and; (III) scissoring in anti-shear. The strain energy release rates and fracture toughnesses in all three modes are usually applied in single-mode criteria or combined in a mixed-mode criterion to determine the onset of propagation, and these generally require curve-fitting parameters taken from experimental testing.

The Virtual Crack Closure Technique (VCCT) is one of the most applied methods for determining the components of the strain energy release rate along a crack front. The VCCT approach was first proposed by Rybicki and Kanninen [5] and is based on two assumptions: 1) Irwin's assumption that the energy released in crack growth is equal to the work required to close the crack to its original length, and; 2) that crack growth does not significantly alter the state at the crack tip. The use of VCCT is advantageous as it allows the strain energy release rates to be determined with simple equations from a single finite element (FE) analysis. Numerous researchers have applied VCCT to analyse the crack growth properties of pre-existing interlaminar damage in a range of structures, including fracture mechanics test specimens [6,7], bonded joints [7,8], and both co-cured and secondary bonded skin-stiffener interfaces [10-12].

Predicting the collapse of a structure taking skin-stiffener separation into account also requires the disbonded area to be grown during the analysis. To date, VCCT has been limited in this respect due to the requirement of a fine mesh of the order of the ply thickness [13] and the need for complicated algorithms to monitor the shape of the crack front. An alternative approach for modelling skin-stiffener separation is with so-called cohesive elements, which are used to control the relationship between opening stresses and displacements in an interface [14,15]. Cohesive elements offer the advantages of incorporating both initiation and propagation of disbonding in such a way that damage is initiated using strength criteria and final separation is governed by fracture mechanics. However, like the VCCT approach, cohesive elements require a fine mesh to remain accurate, and can become prohibitively inaccurate

when larger mesh sizes are used, which makes their application to large structures problematic. Also, the standard cohesive element formulation cannot account for an arbitrary crack front shape and so does not differentiate between mode II and III directions, and in general the exact location of the crack front can be difficult to define. So, in spite of its disadvantages, the VCCT approach remains attractive for application into crack growth analysis as it provides information on the exact nature of the crack front and crack growth mechanisms, and is expected to retain an acceptable degree of accuracy with larger mesh sizes.

In this paper, an approach based on VCCT for handling propagation of interlaminar crack growth in a nonlinear FE analysis is described. This involves modelling the structure with two layers of shell elements separated by a nominal distance and joined using multiple point constraints (MPCs). At the end of every increment, the strain energy release rates are calculated at the MPCs on the crack front using VCCT and accounting for the local crack front directions of an arbitrary crack front shape. Upon satisfaction of simple single-mode criteria the MPC at any failing node pair is released, and the disbonded area is increased for the following increment. Following a description of the modelling approach, numerical results applying the degradation model are then compared with experimental results for a double cantilever beam (DCB) specimen, which is the standard test specimen for determining the mode I fracture toughness G_{IC}. Based on this comparison, recommendations for the future development of the degradation model are made, with reference to improving the apparent conservatism of the VCCT calculation and to adapting the approach to more complex structures.

2 ANALYSIS

In this section, the finite element modelling approach used to represent the separation of two composite layers is first presented. Next, the use of user subroutines to control the growth of the pre-disbonded area throughout the analysis is explained. Then the VCCT equations used to determine the strain energy release rates are given, including the approach for handling an arbitrary crack front. Following this, the crack propagation modelling is discussed, with reference to the assumption of self-similar crack growth.

2.1 Modelling Approach

The modelling approach developed for the separation of two composite layers is given in Figure 1. The structure is modelled as two layers of shell elements separated by a nominal distance, and connected with user-defined MPCs between node pairs. The nodes of the shell elements are located at the interface between the two shells and “dummy” or nominally zero-stiffness layers are used, shown in Figure 2. Placing the nodes at this interface avoids the requirement for complicated constraint equations that would be necessary if the nodes were modelled at the shell mid-planes. The use of dummy layers avoids the use of plate offsets, which can give inaccurate results in geometric nonlinear analyses. This does however introduce an error in the interlaminar shear distribution, as shown in Figure 3, the magnitude of which is proportional to the dummy layer thickness [16]. The nominal distance between the shell layers was set to 0.001 mm, and is required in the fracture mechanics calculation in order to differentiate between opening and closing tying forces in the MPCs. All FE models were analysed with MSC.Marc (Marc), and pre- and post-processed with MSC.Mentat.

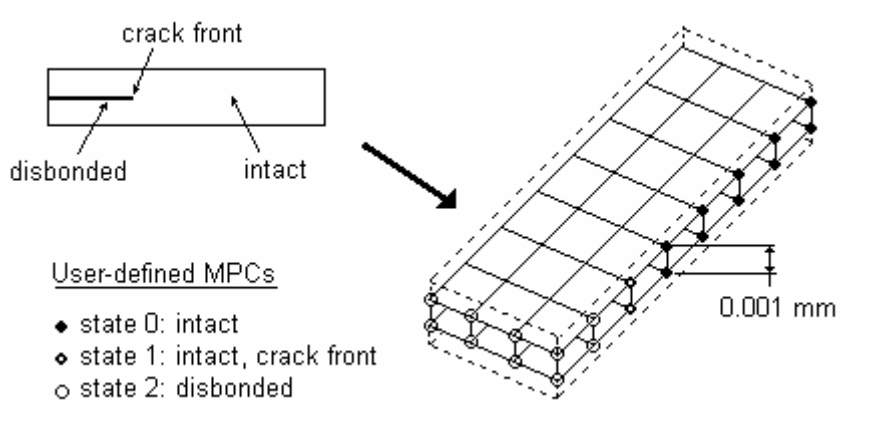

Figure 1: DCB modelling with user-defined MPCs.

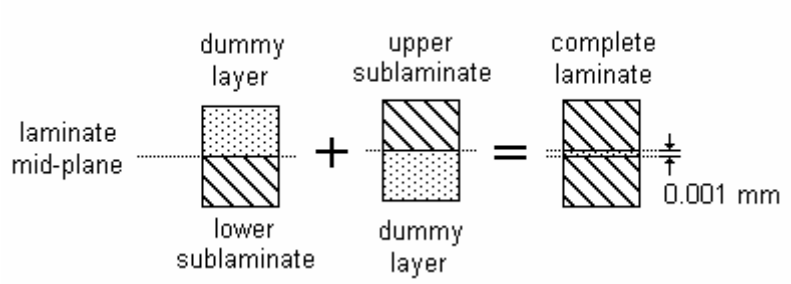

Figure 2: Laminate definition with dummy layers shown.

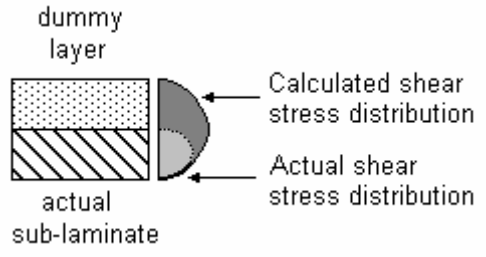

Figure 3: Error in interlaminar shear stress distribution due to dummy layers.

Two user subroutines were written using the UEDINC and UFORMS subroutines provided in Marc [17]. These subroutines are used together to control the MPCs in order to create and grow the disbonded area during an analysis, as illustrated in Figure 4. The user-defined MPCs are given one of three “states”, where state 0 is for MPCs in the intact region, state 1 is for MPCs in the intact region but on the crack front or border between intact and disbonded regions, and state 2 is for MPCs in the disbonded region. The state of each user-defined MPC is kept in an internal variable called a common block, which can be accessed and updated by all subroutines. Each MPC acts on a node pair of one node from each shell layer, with the lower node of each pair arbitrarily selected as the master node. Intact MPCs (states 0 and 1) apply a displacement constraint and disbonded MPCs (state 2) apply no constraint between the two nodes. Note that only the displacements and not the rotations of the nodes are constrained, in order to maintain the correct bending of the separate shell layers. This constraint condition was validated with separate FE models of bending plates containing a disbonded region, and is also in agreement with FE analysis and recommendations of other researchers [10,13].

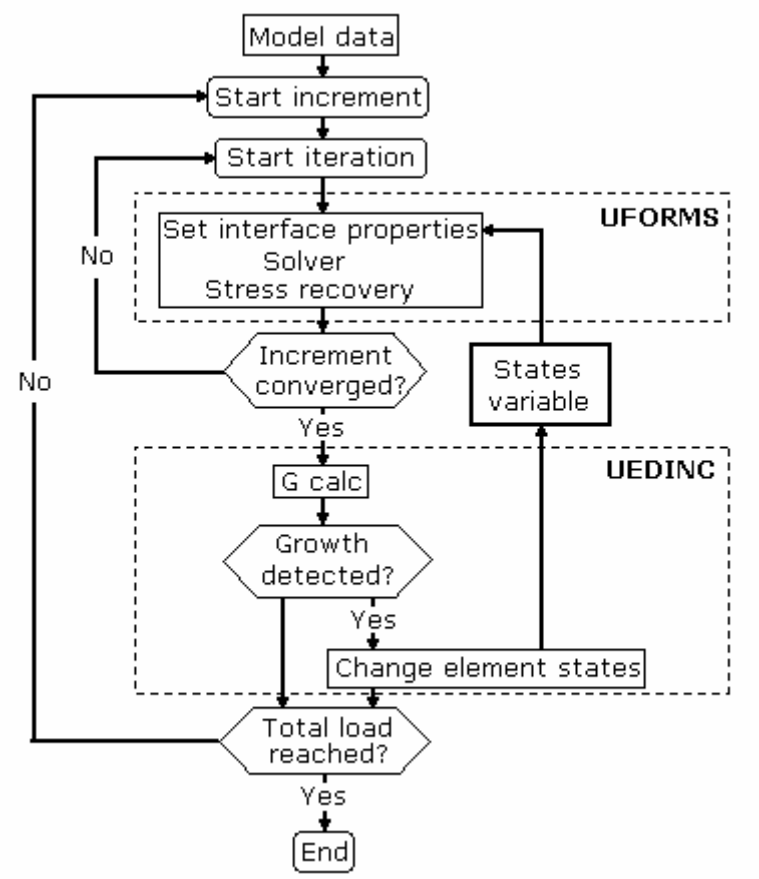

Figure 4: Nonlinear analysis flow with user subroutines for degradation modelling.

The UEDINC user subroutine is a dummy routine provided in Marc that is called at the end of every increment in a nonlinear analysis. With reference to Figure 4, the developed UEDINC subroutine performs a loop over all user-defined MPCs to calculate the strain energy release rates at all MPCs on the disbond front (state 1) and assesses whether the interface fracture toughness has been passed. A separate loop is then used to change the failing MPCs to disbonded (state 2) and to change the corresponding MPCs for the new crack front. The calculation of strain energy release rate is carried out using VCCT equations detailed in the following section.

The UFORMS subroutine is provided within Marc to allow the definition of a user-defined multiple point constraint. The subroutine is called several times in every iteration for each user-defined MPC, and is used to provide the constraint matrix for the calling MPC. The constraint matrix is the matrix that relates the degrees of freedom of the slave node to the master node in the MPC node pair. In the developed UFORMS subroutine the internal state variable is accessed, and the MPC properties are set to either intact for MPC states 0 and 1, or disbonded for MPC state 2.

2.2 Strain energy release rates

The Virtual Crack Closure Technique is based on the Crack Closure Method (CCM) or Two-Step Virtual Crack Closure Technique. In the Crack Closure Method two separate finite element analyses are used before and after the crack is extended, step 1 and 2 as shown in Figure 5 for the two-dimensional case. CCM is based on Irwin's crack closure integral [18],

which assumes that the energy released when the crack is extended is equal to the work required to close it again. From Figure 5, the work to close the crack is found using the force vector, **F**, holding the crack together, taken from step 1, and the displacement vector, $\boldsymbol{\delta}_u - \boldsymbol{\delta}_l$, between the upper and lower nodes when the crack is released, taken from step 2. The energy release rate is equal to the energy released (the work done in closing) divided by the area of crack surface formed, ΔA. This crack surface is the new crack area created as a result of the release of the crack node from step 1 to step 2. In the two-dimensional example of Figure 5, ΔA is equal to $\Delta a \cdot 1$, or the crack growth length multiplied by a unit width, but generally this does not apply, so that the equation for $\Delta \boldsymbol{G}$ or vector change in strain energy release rate is given in Equation 1.

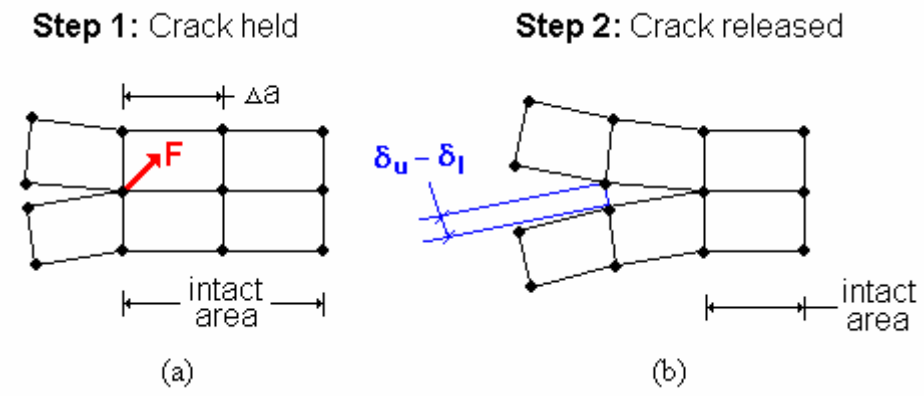

Figure 5: Crack closure method (a) Step 1: Crack closed (b) Step 2: Crack extended.

$$\Delta \mathbf{G} = \tfrac{1}{2}\mathbf{F}\left(\boldsymbol{\delta}_u - \boldsymbol{\delta}_l\right)/\Delta A \tag{1}$$

VCCT is based on the same assumption as CCM of Irwin's crack closure integral. Additionally, it is assumed that crack growth does not significantly alter the state at the crack tip. This means that the displacements ahead of the crack tip in the disbonded area in step 1 can be assumed to be equal to the displacements that will occur when the crack node is released. This allows the calculation to be performed in a single FE analysis, which is particularly relevant here as the calculation is to be included as part of a propagation analysis.

Figure 6 shows a VCCT model created using arbitrary rectangular shell elements, where the upper and lower shell layers in the intact region are overlapping and not distinguishable. To apply VCCT to this type of model the equations need to be modified to account for changes in element length in all directions. From Figure 6, the correct crack surface area needs to be found using the appropriate nodal coordinates. Also, the displacement taken from the node ahead of the crack front needs to be adjusted to account for any difference between the element lengths behind and in front of the crack front. This can be done using linear interpolation, as detailed in Ref. [13] and shown in the last term in the equation below, which gives the modified VCCT equations for use with arbitrary shell elements [10.13]. Note that these equations are for shell elements constrained to each other only by displacements with rotations left free, and as such do not include any rotations or tying moments at the crack front.

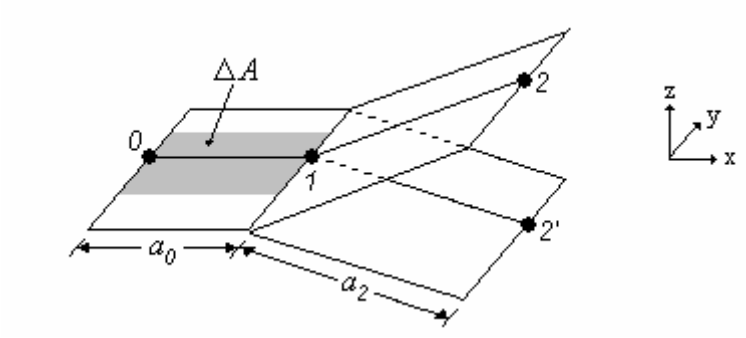

Figure 6: VCCT model with arbitrary rectangular shell elements.

$$
\begin{aligned}
G_I &= -\frac{1}{2}\frac{1}{dA}F_{z1}\left(w_2 - w_{2'}\right)\frac{a_0}{a_2} \\
G_{II} &= -\frac{1}{2}\frac{1}{dA}F_{x1}\left(u_2 - u_{2'}\right)\frac{a_0}{a_2} \\
G_{III} &= -\frac{1}{2}\frac{1}{dA}F_{y1}\left(v_2 - v_{2'}\right)\frac{a_0}{a_2}
\end{aligned}
\tag{2}
$$

where, with reference to Figure 6: G_I, G_{II}, G_{III} are strain energy release rates in local mode I, II and III directions; ΔA is the virtual crack growth area; $\{F_x, F_y, F_z\}$, and $\{u, v, w\}$ are forces and displacements in the local x, y and z directions; a are distances from the crack front MPC; subscripts 0, 1 and 2 refer to values taken from MPCs of states intact crack front and disbonded respectively, and; 2' is the lower node of the MPC in the disbonded region.

Also critical for the application of VCCT to an arbitrary crack front is the determination of the local crack front directions. The method for determining the local crack front coordinate system was adapted from Ref. [13], and is illustrated in Figure 7. Important in this approach is the determination of the neighbouring nodes along the crack front, which are used to form the local mode III direction and to determine the local mode I and II directions using cross products. With the local crack front coordinate system the forces and displacements can be resolved into their correct mode I, II and III components, to reflect the true crack opening mechanisms acting locally on the crack front.

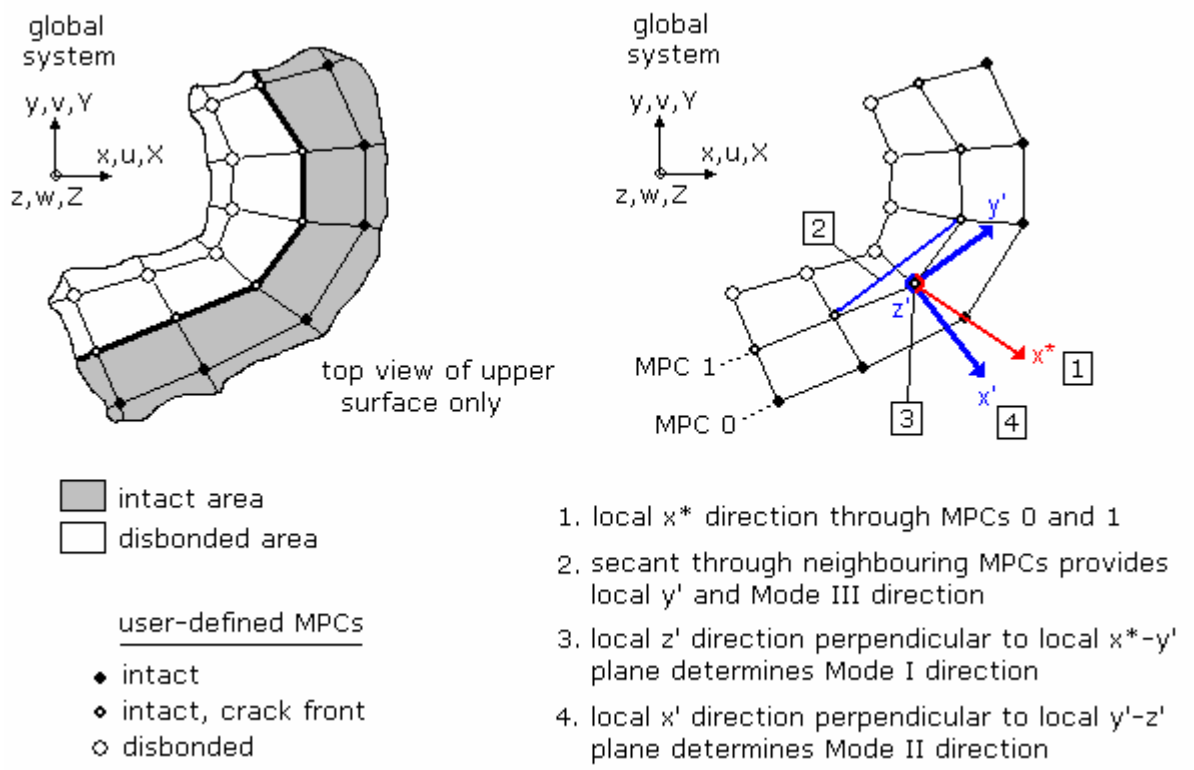

Figure 7: Determining the local crack front coordinate system for an arbitrary crack front, adapted from [13].

In order to apply the VCCT approach in a propagation analysis it is necessary to account for the wide variety of crack front shapes possible, shown in Figure 8. Whilst all of these crack shapes are not expected in the DCB model, for more complex models it is necessary to account for all crack growth possibilities. From this figure, any crack front shape or crack type is considered to be defined in the centre of a maximum of four 4-noded shell elements, that is any crack front MPC can have a maximum of four adjacent side MPCs and four diagonal MPCs. Crack types are classified according to the status of the adjacent side MPCs, and whether the MPC is on a structural edge. It is assumed that triangular elements are not used.

The VCCT calculation requires the assumption of self-similar growth, as previously described. For the variety of different crack front shapes, crack growth is assumed to be "locally self-similar". This means that crack growth will involve propagation of the entire local crack front shape, and is a necessary assumption in order to determine the correct displacements and areas necessary for the VCCT calculation. Though alternative assumptions of crack propagation are possible, the self-similar assumption is the classic VCCT assumption, and it is expected to provide conservative solutions. The only exception to this was for crack growth at a convex corner, crack type 10 in Figure 8, where self-similar crack growth was deemed to be unrealistic in this instance. The accuracy of the self-similar assumption and its implications for the propagation of the crack front are discussed in the following section. The choice of displacements and areas for each crack type is given in Figure 8, where in the "VCCT MPCs" column, the "displacements" MPC is the one from which displacements are taken, and the "new location" MPC is the one to which the central failing MPC is grown.

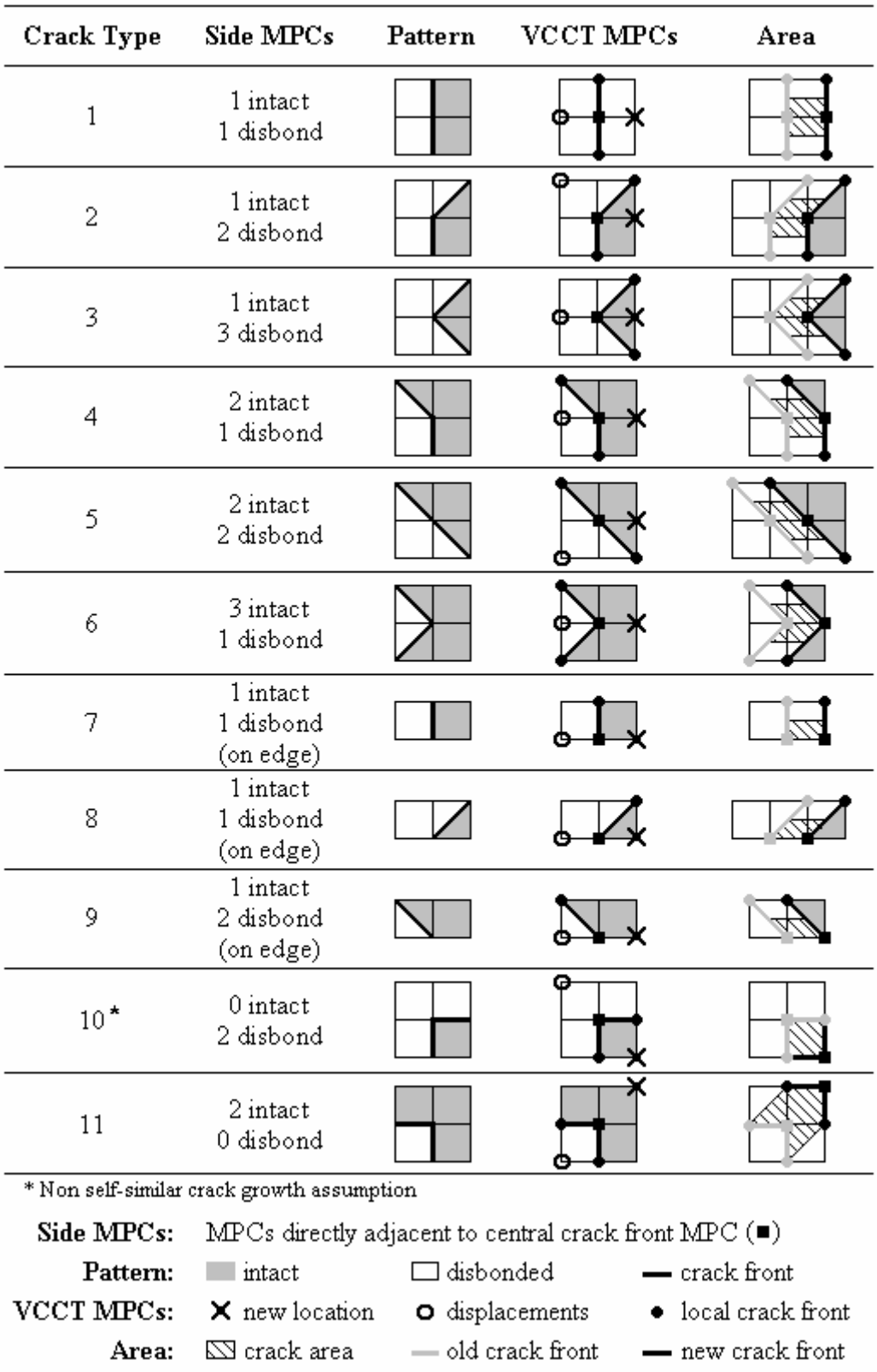

Figure 8: Crack front pattern, VCCT MPCs and crack growth area for each crack growth type.

2.3 Propagation Modelling

The propagation method is the way in which the crack front is advanced once failure is deemed to have occurred. The propagation method implemented is illustrated in Figure 9,

where the VCCT calculation is performed at every crack front MPC, "failure" is where the crack growth criteria have been satisfied at an MPC, and "release" of an MPC is a change to the disbonded state 2. In this approach, each failing MPC is released, and the adjacent intact MPCs are modified to become crack front MPCs. It should be noted that this type of crack propagation is not made with any reference to the VCCT calculation, and as a result of this the assumption of self-similar growth can be violated. Examples of this are given in Figure 9 for a simplified DCB specimen with large elements, where one and two elements fail, and the crack front in the next increment does not correspond to the crack front for self-similar growth. So, the displacement that occurred once the MPC was released is less than the displacement that was assumed from the straight crack front, and the energy released in crack growth was overestimated. However, for DCB specimens, it is common that the strain energy release rates are nearly constant along the majority of the crack front, with the exception of the edges, at which the strain energy release rates are much less [19]. So, in spite of its conservatism this approach is still applicable for DCB specimens.

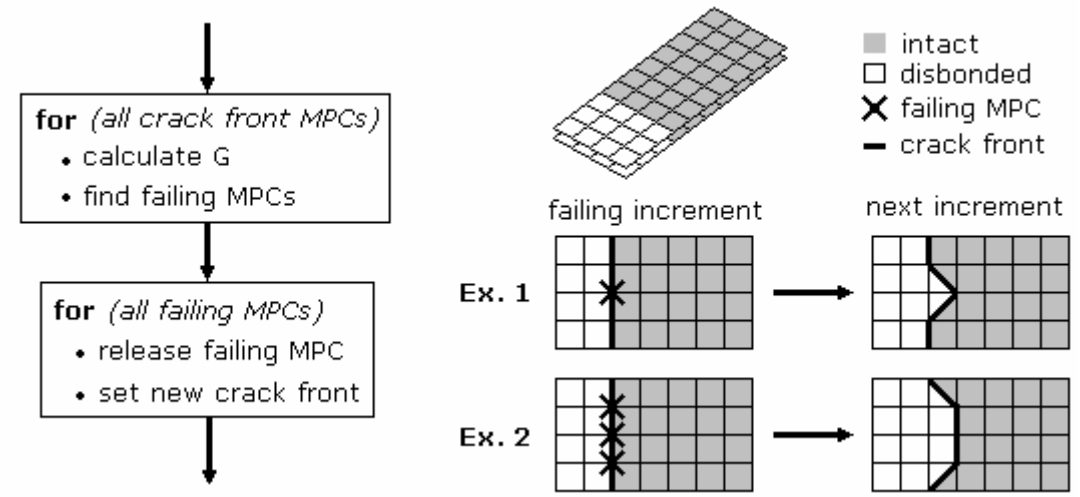

Figure 9: Analysis flow and example growth showing the propagation method.

3 RESULTS AND DISCUSSION

In this section, experimental results for a double cantilever beam are presented and are compared to numerical analyses using the degradation model described above. This is followed by discussion on the quality of the comparisons, the accuracy and efficiency of the propagation model, and the functionality and future development of the degradation model.

3.1 Experimental Results

To determine the mode I fracture toughness of the unidirectional carbon fibre prepreg material IM7/8552, tests were performed on a series of DCB specimens at the DLR [20]. The tests were performed in accordance with the German standard [21], and details of the specimen and material are given in Table 1, where in the material lay-up "//" is used to denote the location of the delamination in the pre-cracked region. Note that in contrast to the completely unidirectional laminate specified in the standard, a multi-directional laminate was used, as large blocks of unidirectional plies are rarely applied in aerospace design. A quasi-isotropic lay-up was used that was symmetric about the central 0°/0° interface, to minimise the additional anti-clastic curvature caused by the use of a multi-directional laminate, according to the recommendations given in Ref [19].

Length	250 mm
Width	25 mm
Teflon insert	25 mm × 25 mm × 0.02 mm
Crack extension from pre-load *	25 mm
Total pre-crack length *	50 mm
Layup	$[(0,90,+45,-45)_{2S}$ // $(0,90,+45,-45)_{2S}]$
Ply thickness	0.152 mm
Total thickness	4.864 mm

* Approximate value taken from DCB Test #7

Table 1: Geometry and material specifications for DCB experimental tests.

Nine DCB specimens were manufactured using a Teflon insert to generate a delamination at the central 0°/0° interface. The specimens were loaded by pulling down on one of the delaminated edges, with the other delaminated edge rigidly held and pin supports used on the non-delaminated edge. Hinged plates were bonded to the delaminated edges to assist with load introduction. For each test, the applied load and loading displacement was available from the testing machine as output, and this was used to calculate the critical strain energy release rate. The test procedure involved pre-loading the structure to create a "natural" crack front from the edge of the Teflon insert. The pre-load was then removed, and the specimen was loaded until the total crack length was approximately 100 mm. A typical load-displacement graph is given in Figure 10 for specimen #7, which also includes the fracture toughness obtained for this test. As this fracture toughness was very close to the average fracture toughness of all specimens, the load-displacement and fracture toughness obtained from this test were used to compare with the numerical analyses. For specimen #7, crack growth was initiated at an applied displacement of around 1.5 mm, or 106 N, and the loading was stopped at an applied displacement of around 13.2 mm, at which the crack had grown from an initial length of 49.2 mm to 127.4 mm.

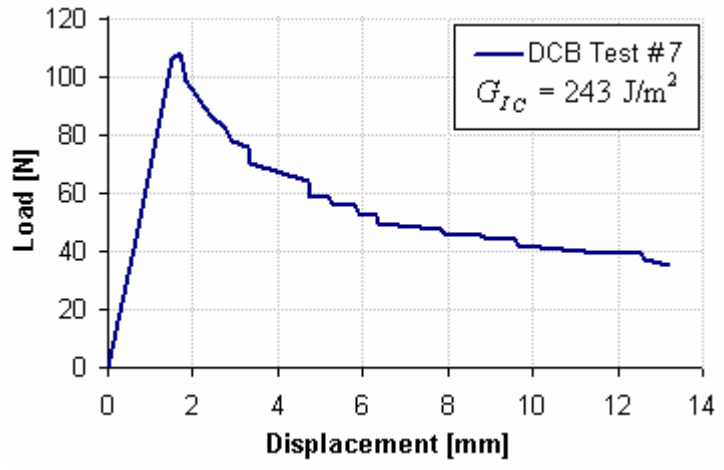

Figure 10: Applied load versus displacement for DCB Test #7, with resultant fracture toughness value also given.

3.2 Numerical Analysis

Finite element models were generated according to the modelling approach and the specimen characteristics of Table 1. An overview of the modelling is given in Figure 11, in which the hinge modelling and boundary condition (BC) definition are also given. The four mesh

densities used were characterised according to the element length in the crack growth direction, 5 mm, 2.5 mm, 1.25 mm and 0.125 mm, and consisted of respectively 500, 936, 3460 and 5856 four-node bilinear thick-shell elements. The 0.125 mm model was created in accordance with Ref. [13], in which element lengths between 0.1 and 1.0 times the ply thickness are recommended with VCCT. Results from the 0.125 mm model were used to assess the errors involved using larger elements at crack growth initiation only, so only a crack growth region of five elements (0.625 mm) was modelled. The 5 mm model used all square elements, and the other models used square elements of the characteristic length in the crack growth region followed by a mesh transition scheme to larger elements. The mesh transition scheme avoided the use of triangular elements and ratios between the largest and smallest side lengths greater than 3, with an example given in Figure 12. The user-defined MPCs were applied in a region extending up to a maximum possible crack length of 150 mm, based on the total crack growth in the experiment. For the rest of the specimen, standard pin jointed MPCs were used to constrain the displacements of the upper and lower sublaminates. For each model the hinge and load application were defined as shown in Figure 11, where edges of the specimen bonded to the hinge plates were modelled as a rigid region, and the hinges were modelled as single nodes that constrained only the displacements of the attached structure. Though the hinge dimensions were based on the hinges used in the experiment, modifications were made in order to get good agreement with the initial experimental stiffness, which was necessary so that the hinge modelling did not affect the comparison of crack growth prediction.

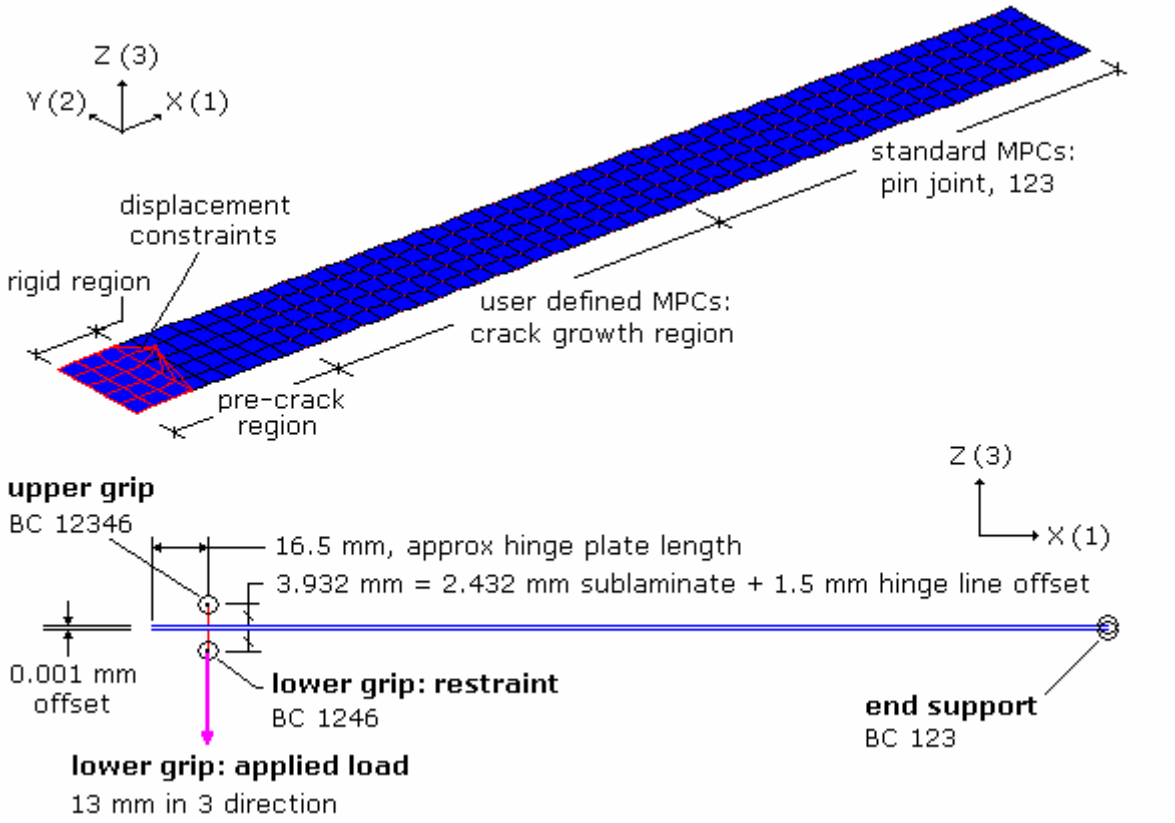

Figure 11: DCB modelling overview (5 mm model shown), with hinge modelling and boundary conditions.

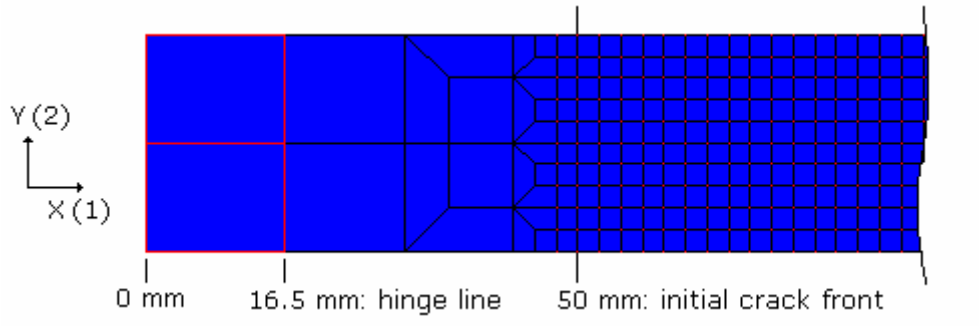

Figure 12: Detail of the mesh transition scheme, 2.5 mm model shown.

All models were analysed using the nonlinear solver in Marc, which applied a full Newton-Raphson procedure and the Marc default convergence tolerance of 0.1 on load residuals. The 0.125 mm model encountered convergence problems due to the large number of MPCs released between increments affecting the energy balance of the structure, so for this model a relative displacement criterion with tolerance of 0.1 was included as an alternative to the load residuals. The 5 mm, 2.5 mm and 1.25 mm models were each run with 13 mm applied displacement load, and the 0.125 mm model was only run to an applied displacement of 1.4 mm. Analysis results are presented below, where Figure 13 is the applied load versus displacement, Figure 14 is the strain energy release rate before any crack growth, Figure 15 gives an example of the final deformed shape and Figure 16 illustrates the crack progression, where "applied disp" is the applied displacement for each crack front pattern shown. Table 2 is a summary of all analysis runs, where δ_{init} is the displacement at crack growth initiation, P_{max} is the maximum load, a_{max} is the final crack length, t is the total analysis time, inc is the total number of increments, and t_{avg} is the average time per increment.

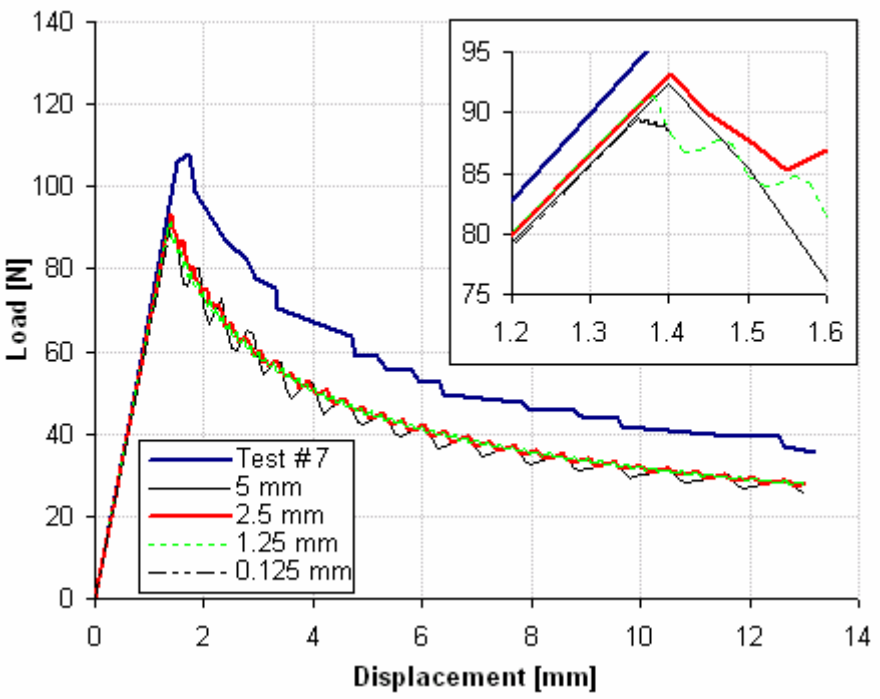

Figure 13: Applied load versus displacement for all models with close-up view of propagation initiation region.

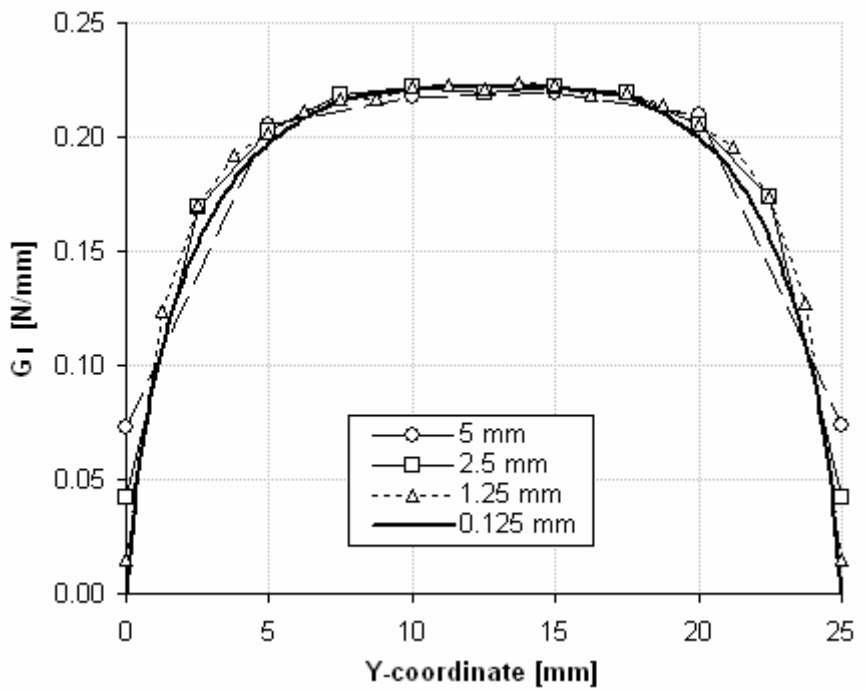

Figure 14: Mode I strain energy release rate at 1.3 mm applied displacement (before crack growth), all models.

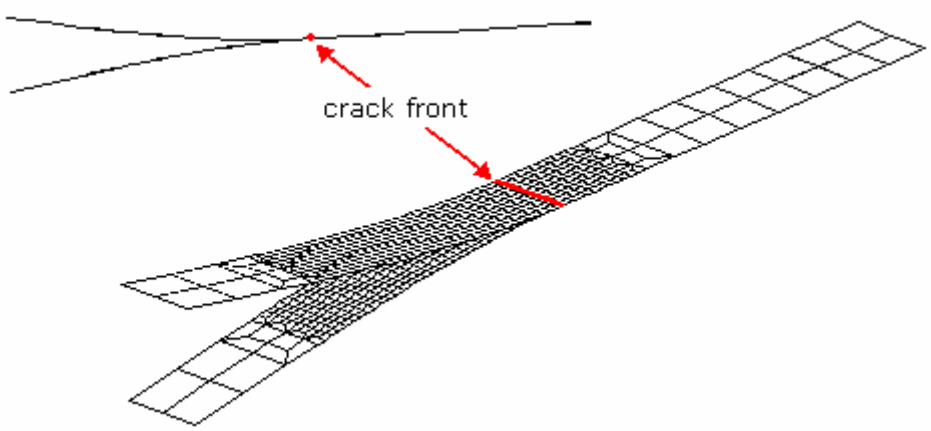

Figure 15: Final deformed shape at 13 mm applied displacement, 2.5 mm model.

Model	δ_{init} [mm]	P_{max} [N]	a_{max} [mm]	t [hr]	inc	t_{inc} [s]
5 mm	1.4	92.4	130	0.57	121	16.9
2.5 mm	1.4	93.2	127.5	1.69	235	25.9
1.25 mm	1.36	91.4	128.75	16.0	586	98.4
0.125 mm	1.36	–	–	1.84*	51	129.7
Experiment	1.52	108	127.4	–	–	–

* Analysis was only run to 1.4 mm of 13 mm total displacement

Table 2: FE analysis summary, all models.

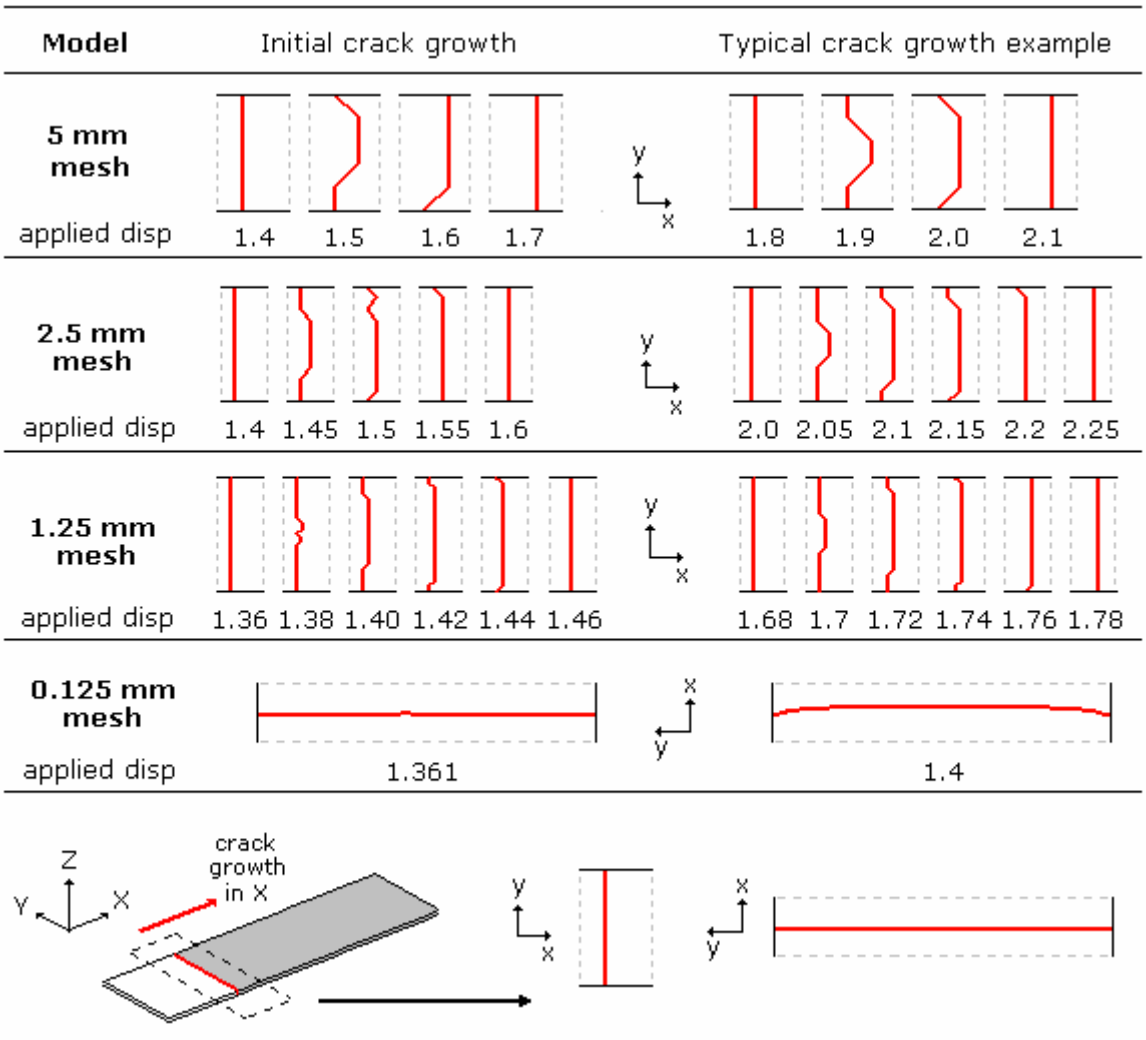

Figure 16: Examples of crack progression for all models, applied displacements in mm.

All FE models gave close comparison with the experimental results, with the structural and crack propagation behaviour accurately represented. The final crack length values gave excellent comparison with the experiment and appeared independent of the mesh density. Though comparing well with the experimental values, the load-displacement results did appear to show a degree of underestimation or conservatism for all models that remained constant for all analyses. For the 5 mm, 2.5 mm and 1.25 mm models, the crack advanced as a straight crack, and alternated between a stationary full width straight crack and a jagged crack front in crack growth. This behaviour was reflected in the "saw-tooth" appearance of the load-displacement graph, where in general the straight and jagged crack fronts corresponded to increasing and decreasing load-displacement behaviour respectively. The sequence of failing MPCs along the crack front was usually identical between growth steps for each different mesh density, and this sequence was more or less symmetrical for all models. The 0.125 mm model showed crack propagation in a thumbnail shape, though the load-displacement values showed very close agreement with the other mesh density models. The thumbnail crack front shape is a phenomenon for DCB specimens that is well known both theoretically and experimentally, and is due to the anti-clastic curvature of the structure [19,22].

Comparing the different mesh density models, there were differences in both the crack propagation shapes and strain energy release rate distributions. Increasing the element size increased the strain energy release values, most noticeably at the panel edges, at which there was considerable variation between the models. In spite of these differences, the results indicate that the mesh density did not affect the overall structural response and crack propagation behaviour, which is seen from the very similar behaviour of all numerical models.

Concerning analysis time, the mesh density was critical, both in terms of the obvious increase in computational expense, but also importantly it was found that the mesh density dictated the appropriate increment size. The increment size needed to be small enough so that the crack opening between increments did not significantly outpace the crack growth. The use of large increments with small elements did not allow the structure to propagate the crack fast enough, and the material behaviour would be overestimated. For this reason the 5 mm, 2.5 mm, 1.25 mm and 0.125 mm models used increments sizes of 0.1 mm, 0.05 mm, 0.02 mm and 0.001 mm, respectively. The steep rise in total analysis time as a result of the both of these effects can be seen in Table 2, where the t_{inc} value is an attempt to normalise the analysis times. Whilst this does not account for the varying number of iterations within an increment, it does give a more realistic appreciation of the relationship between model size and computational expense than the total analysis time.

3.3 Discussion

The comparison between numerical and experiment results have shown the VCCT calculations to be conservative. As was mentioned previously, this conservatism arises from the relationship between the assumptions made in the VCCT calculation and the actual crack front that is created in the following increment. When the displacements of the nodes that are released are less than the displacements that were assumed for the VCCT calculation, then less energy is being released in crack growth than the material should be able to support, and the material fracture toughness is underestimated. For the DCB specimen, it was expected that this would not be too inaccurate as DCB crack fronts typically show mostly constant strain energy release distributions, and this behaviour was seen in the numerical results presented. However, for more complicated structures and crack front shapes the conservatism of the VCCT approach needs to be investigated.

In order to address this conservatism, it is necessary to account for the relationship between the assumptions in the calculation and actual crack front shape propagated. One option for this is to force crack growth in accompanying areas when an MPC is released, in such a way that the local crack front shape is conserved. Similarly, another option would be to advance the entire crack front upon failure at any location. Both of these options would attempt to force the states at the crack front before and after growth to be similar, though both could lead to further conservatism as they involve forcing growth on regions of the crack that have not failed. Another approach would involve modifying the values of strain energy release calculated to account for the difference between the assumed and the actual crack front shape. This would require an understanding of the difference in displacements resulting from different crack shapes, of which the large variation available may prohibit an effective approach. An investigation into various propagation models is the focus of current studies, and these have indicated that the latter approach can produce more accurate results, though may require parametric studies in order to understand the relationship between MPC release and the subsequent deformation shape.

The results presented indicate that the VCCT approach can remain accurate for large mesh sizes, and can be used to make predictions on the load-carrying capacity and structural response. This is important in terms of the development of the degradation model with respect to the goal of capturing structural degradation of large fuselage-representative structures. So, whilst a fine mesh will generally always be necessary if detailed information on the crack initiation and crack shapes is required, the results indicate that the developed approach is suitable for capturing the effect of skin-stiffener separation on the overall response. It must be noted that many researchers have found VCCT to give mesh-dependent results, especially for the so-called "bi-material" interface between two dissimilar sublaminates [13]. However, there are approaches that can be applied to handle this, which include performing mesh densities studies to understand the extent of any influence, and comparing results with those obtained from an adequately fine mesh, both of which were demonstrated in this paper.

Future development of the degradation model will focus on the apparent conservative nature of the VCCT. This will involve the investigation of a number of different propagation methodologies, in order to develop an approach in which the strain energy release rate calculation and the subsequent crack propagation are based on the same crack front state. Separately, the degradation model presented in this paper will be developed further in order to be applicable to more complex structures. This will involve the use of contact elements to prevent interpenetration in the disbonded region, and the prediction of the initiation of skin-stiffener disbonding from an intact structure. Furthermore, an additional degradation model will be developed to represent the damage mechanisms of the fibre and matrix on the ply-level. Importantly, the development of these various degradation models will also benefit from the large amount of testing carried out within the COCOMAT project, which includes structures ranging from material characterisation and fracture mechanics tests to large multi-bay curved stiffened panels both with and without various damage types. The application of the degradation models to these experimental results will be critical for the development, validation and demonstration of the proposed degradation modelling approach.

4 CONCLUSION

A degradation model was proposed for capturing the propagation of skin-stiffener separation in composite stiffened panels as part of the European Commission Project COCOMAT. The degradation model was implemented for nonlinear finite element analysis using two user subroutines in MSC.Marc. In the developed approach, user-defined multiple point constraints were applied to control the connection of two shell element layers. At the end of every increment, fracture mechanics calculations were performed using the VCCT and any failing MPCs were released for the next increment. In this way, the disbonded area could be grown during an analysis and the resultant structural degradation due to disbonding represented.

Numerical predictions using the degradation methodology were compared to experimental results for a double cantilever beam specimen. Close comparison was observed for all aspects of structural behaviour, which included the load-carrying capacity, structural deformation and crack propagation. Significantly, it was shown that the use of VCCT with relatively large elements gave almost identical results to even a ply-thickness element length model, and that the use of smaller elements was doubly disadvantageous for computation time as it also required the use of small increment sizes. The results did indicate a degree of conservatism in the VCCT calculation, and it was concluded that this was due to the relationship between the assumption of self-similar growth in the calculation and the actual crack front propagated.

Recommendations were made for the future development of the degradation model, with reference to improving this apparent conservatism and to the application of the method to other specimen types and stiffened structures representative of composite fuselage designs.

5 ACKNOWLEDGEMENTS

The authors kindly acknowledge the support of: the European Commission, Priority Aeronautics and Space, Contract AST3-CT-2003-502723; the Australian Postgraduate Awards Scheme; the German Academic Exchange Service, the Italian Ministry of Foreign Affairs, and; the Australian Government under the "Innovation Access Programme – International Science and Technology". The authors would also like to acknowledge the generous assistance of Dr Michael Giess of MSC.Software Australia and also Prof. Murray Scott of the CRC-ACS for support within the COCOMAT project.

REFERENCES

[1] R. Degenhardt, R. Rolfes, R. Zimmerman and K. Rohwer, COCOMAT – Improved **MAT**erial Exploitation at Safe Design of **CO**mposite Airframe Structures by Accurate Simulation of **CO**llapse, *Composite Structures*, **73**, 175-178, 2006.

[2] COCOMAT Home Page, www.cocomat.de, 2006.

[3] T. K. O'Brien, Characterization of delamination onset and growth in a composite laminate. *Damage in Composite Materials*, ASTM STP 775, 140–167, 1982.

[4] T. K. O'Brien, Interlaminar fracture toughness: The long and winding road to standardization. *Composites: Part B*, **29**, 57–62, 1998.

[5] E. F. Rybicki and M. F. Kanninen, A finite element calculation of stress intensity factors by a modified crack closure integral. *Engineering Fracture Mechanics*, **9**, 931–938, 1977.

[6] R. Krüger, M. König and T. Schneider, Computation of local energy release rates along straight and curved delamination fronts of unidirectionally laminated DCB- and ENF-specimens. *34th AIAA/ASME/ASCE/AHS/ASC SSDM Conference, La Jolla, CA*. AIAA Washington, 1332–1342, 1993.

[7] J. Li, S. M. Lee, E. W. Lee and T. K. O'Brien, Evaluation of the edge crack torsion ECT Test for mode III interlaminar fracture toughness of laminated composites. *Journal of Composites Technology and Research*, **19**, 174–183, 1997.

[8] M. M. A. Wahab, On the use of fracture mechanics in designing a single lap adhesive joint. *Journal of Adhesive Science and Technology*, **19**, 851–865, 2000.

[9] M. Qin and Y. Dzenis, Nonlinear numerical and experimental analysis of single lap adhesive composite joints with delaminated adherends. *13th International Conference on Composite Materials (ICCM13)*, Y. Zhang, ed., Beijing, 2001.

[10] J. T. Wang and I. S. Raju, Strain energy release rate formulae for skin-stiffener debond modeled with plate elements. *Engineering Fracture Mechanics*, **54**, 211–228, 1996.

[11] J. Li, T. K. O'Brien and C. Q. Rousseau, Test and analysis of composite hat stringer pull-off test specimens. *Journal of the American Helicopter Society*, 350-357, 1997.

[12] W. S. Johnson, L. M. Butkus and R. V. Valentin, *Applications of Fracture Mechanics to the Durability of Bonded Composite Joints*. U.S. Department of Transportation, Federal Aviation Administration DOT/FAA/AR-97/56, 1998.

[13] R. Krueger, *The Virtual Crack Closure Technique: History, Approach and Applications*. NASA/CR-2002-211628, ICASE Virginia, USA, 2002.

[14] P. P. Camanho and C. G. Dávila, *Mixed-mode Decohesion Finite Elements for the Simulation of Delamination in Composite Materials*. NASA/TM-2002-211737, NASA Langley Research Center, Virginia, USA, 2002.

[15] Y. Mi, M. A. Crisfield and G. A. O. Davies, Progressive delamination using interface elements. *Journal of Composite Materials*, **32**, 14, 1246–1272, 1998.

[16] J. W. H. Yap, R. S. Thomson, M. L. Scott and D. Hachenberg, Influence of post-buckling behaviour of composite stiffened panels on the damage criticality. *Composite Structures*, **66**, 197–206, 2004.

[17] *MSC.Marc Volume D: User Subroutines and Special Routines*, MSC.Software Corporation, California, USA, 2004.

[18] G. R. Irwin, Fracture I. *Handbook der Physik*, Flügge, ed., pp. 558-590, 1958.

[19] B. D. Davidson, An analytical investigation of delamination front curvature in double cantilever beam specimens. *Journal of Composite Materials*, 24, 1124–1137, 1990.

[20] Kling A., Degenhardt, R., Characterization of material properties – Results of the EU project COCOMAT. *Internal DLR Report*, IB 131-2006/18, April 2006.

[21] *Determination of Interlaminar Fracture Toughness Energy – Mode I – G_{IC}*. European Normative Standard DIN EN 6033, Deutsches Institut für Normung, e. V., 1996.

[22] A. J. Brunner, Experimental aspects of Mode I and Mode II fracture toughness testing of fibre-reinforced polymer-matrix composites. *Computational Methods in Applied Mechanics and Engineering*, **185**, 161-172, 2000.